Journal of the Mechanics and Physics of Solids 129 (2019) 229–243

Contents lists available at ScienceDirect

Journal of the Mechanics and Physics of Solids

journal homepage: www.elsevier.com/locate/jmps

Isotropic polar solids for conformal transformation elasticity and cloaking

H. Nassar, Y.Y. Chen, G.L. Huang*

Department of Mechanical and Aerospace Engineering, University of Missouri, Columbia, Missouri 65211, USA

ARTICLE INFO

Article history:
Received 11 March 2019
Revised 3 May 2019
Accepted 3 May 2019
Available online 4 May 2019

Keywords:
Polar elasticity
Conformal transformations
Cloaking
Stress symmetry
Chirality
Hexachiral lattices

ABSTRACT

The paper initiates a constitutive theory of isotropic linear elastic solids where Cauchy's stress tensor is not necessarily symmetric thus earning them the attribute "polar". Mainly, expressions for the fourth-order elasticity tensors of isotropic polar solids in two and three space dimensions are derived. It is found that the constitutive tensors feature, in addition to the usual bulk and shear moduli, one extra independent elastic constant in 3D, and two extra constants in 2D. In the latter case, the new constants quantify to which degree stress and mirror symmetries are broken. Indeed, it turns out that in 2D, stress asymmetry enables isotropic yet chiral behaviors and the interplay between chirality and polarity is subsequently investigated.

To motivate the theory, it is shown that 2D isotropic polar solids naturally arise in the application of the transformation method when the background medium is isotropic and when the underlying spatial transformation is conformal (i.e., angle-preserving). Accordingly, isotropic polar solids, in conjunction with conformal transformations, can simplify the design of invisibility cloaks and other wave-steering devices by circumventing the need for anisotropic behaviors. As a demonstration, a conformal carpet cloak is designed out of graded hexachiral lattices and numerically tested. The cloaking performance is shown to be satisfactory over a range of pressure-shear coupled dynamic loadings.

© 2019 Elsevier Ltd. All rights reserved.

1. Introduction

The transformation method (Greenleaf et al., 2003a,b) is a powerful tool for the design of structures that guide waves in specific purposeful manners. Indeed, there exist transformation rules dictating what gradients of material properties are needed in order to spatially transform and rearrange the fields that reign within a domain. The study of these spatial transformations as well as the associated transformation rules for light and sound constitutes what has become known as transformation optics and acoustics. Cloaking, the most notorious application of the transformation method, is undoubtedly responsible for kindling research interest in these areas (Leonhardt, 2006; Pendry et al., 2006). But cloaking related or not, the method is not without its difficulties. Most notable is the fact that when the original domain, i.e., pre-transformation, is isotropic, the constitutive materials of the image domain, i.e., post-transformation, turn out to be anisotropic in general.

* Corresponding author.
E-mail addresses: nassarh@missouri.edu (H. Nassar), yc896@mail.missouri.edu (Y.Y. Chen), huangg@missouri.edu (G.L. Huang).

https://doi.org/10.1016/j.jmps.2019.05.002
0022-5096/© 2019 Elsevier Ltd. All rights reserved.

Designing gradients of anisotropic materials can be challenging yet ultimately proved possible in several important cases pertaining to cloaking against acoustic waves in fluids (Chen and Chan, 2007; Cummer and Schurig, 2007; Norris, 2008; 2015), flexural waves in plates (Brun et al., 2014; Chen et al., 2016; Colquitt et al., 2014; Farhat et al., 2009a, 2012, 2009b; Norris, 2015; Stenger et al., 2012) and against more general elastic waves in solids (Nassar et al., 2018; Norris and Parnell, 2012; Parnell, 2012; Parnell et al., 2012).

In the case of elasticity and in contrast to optics and acoustics, spatial transformations are not only susceptible of changing the material symmetry of the constitutive tensors but also their index symmetries (Brun et al., 2009; Diatta and Guenneau, 2014; Milton et al., 2006; Norris and Shuvalov, 2011). Namely, the image elasticity tensor **a** turns out to generally violate the minor index symmetries $a_{ijkl} = a_{jikl} = a_{jilk}$. In other words, the image domain tolerates asymmetric stresses; we qualify such domains as "polar". With that in mind, it is the purpose of this paper to provide a constitutive theory of isotropic polar solids thus laying the foundations of an isotropy-preserving transformation method.

Several theories of elasticity with asymmetric stresses are possible, including the one by the Cosserat brothers (1909) also known as micropolar elasticity (Cemal Eringen, 1999; Maugin, 1998). As a matter of fact, the polar theory proposed hereafter can be seen as a version of micropolar elasticity simplified and modified to fit the requirements of the transformation method. First, starting with the full theory, microrotation is dismissed, one way or another, to obtain what the literature refers to as the couple stress theory (Hadjesfandiari and Dargush, 2011; Mindlin, 1963; Mindlin and Tiersten, 1962; Toupin, 1964). Second, we neglect couple stresses but not body torque. Third, we assume that body torque is linearly dependent on deformations. Fourth, we embed torque equilibrium into Hooke's law. The outcome of this process is what we refer to as polar elasticity. In doing so, the elasticity tensor gains extra freedom as its asymmetric components no longer need to vanish. Specifically, under the assumption of isotropy, it is found that the elasticity tensor features, in addition to the usual bulk and shear moduli, one extra independent elastic constant in 3D, and two extra constants in 2D. In the latter case, the new constants quantify to which degree stress and mirror symmetries are broken. Indeed, it turns out that 2D polar elasticity enables isotropic yet chiral behaviors.

In order to illustrate the usefulness of the suggested theory in 2D, we show that an isotropy-preserving transformation method is possible if spatial transformations are restricted to conformal ones, i.e., to transformations that locally conserve angles. The corresponding transformation rules then dictate that the image domain is composed of a gradient of isotropic polar materials (*i*) with the same shear modulus as the original domain; (*ii*) with bulk, polarity and chirality moduli depending solely on the original bulk modulus as well as on the local angle of rotation of the conformal transformation; (*iii*) that are degenerate, in that they admit a stressless strainful deformation mode. It should be noted that conformal transformations have been known to preserve the isotropy of optical and acoustic properties (Leonhardt, 2006; Norris, 2012; Xu and Chen, 2014); the present work extends these efforts to the case of elasticity and resolves the complications related to the loss of the minor symmetries.

As an application, a lattice design of a conformal cloak of the "carpet" variety is proposed following ideas by Leonhardt (2006) and by Li and Pendry (2008). Carpet cloaks can render invisible objects placed along an interface, e.g., a free boundary. The cloak's design is found in two steps. In the first step, spring-mass lattices whose behavior in the homogenization limit can target that of the constitutive materials of the cloak are parametrized. Aiming for a chiral yet isotropic behavior, the adopted lattices are based on an adaptation of the well-known hexachiral lattices (Auffray et al., 2010; Bacigalupo and Gambarotta, 2014; Chen et al., 2014; Frenzel et al., 2017; Liu et al., 2012; Rosi and Auffray, 2016; Spadoni and Ruzzene, 2012; Spadoni et al., 2009). In the second step, the derived transformation rules are used to solve for the lattice parameters at each position in the domain of the cloak. The lattice cloak is subsequently tested numerically under combined pressure and shear dynamic loads and at various angles of incidence with the simulations showing approximate but satisfactory cloaking performance.

The rest of the paper goes as follows. The second section presents a theory of linear elastic polar solids. Therein, we derive general expressions for the constitutive tensors, account for the extra independent elastic constants they exhibit and investigate the interplay between polarity, chirality and degeneracy in basic yet insightful static and dynamic load cases. In the third section, a theory of conformal transformation elasticity is proposed and transformation rules relating the elastic properties of the original and image domains are derived. Then, in the fourth section, a lattice carpet cloak is designed and tested. The last section contains a brief conclusion.

2. Isotropic polar solids

In what follows, we investigate the linear elastic behavior of isotropic polar solids. We calculate general expressions for isotropic fourth-order elasticity tensors that exhibit the major index symmetry but not necessarily the minor ones and account for the extra independent elastic constants needed for their description. For later purposes, emphasis is given to the conditions under which the behavior is degenerate. Degeneracy and polarity are in fact main byproducts of spatial transformations but the connection to the transformation method is left for the next section. Meanwhile, in 2D, we show that polar solids are chiral in general and deduce some of the salient symptoms of chirality in statics and dynamics.

2.1. Governing equations

Within the context of infinitesimal deformations, we define a linear elastic polar solid as one governed by Cauchy's law of motion

$$\sigma_{ij,j} + \rho f_i = \rho \dot{v}_i, \tag{1}$$

and whose strain energy $\psi = \psi(\mathbf{e})$ is quadratically dependent over the displacement gradient $\mathbf{e}$. Therein, $\boldsymbol{\sigma}$ denotes the stress tensor, ρ is mass density, $\mathbf{f}$ is body force and $\mathbf{v}$ is particle velocity.

Hooke's law is obtained by differentiation and reads

$$\sigma_{ij} = \frac{\partial \psi}{\partial e_{ij}} = a_{ijkl} e_{kl}. \tag{2}$$

Since $\mathbf{a}$ derives from ψ, it satisfies the major index symmetry $a_{ijkl} = a_{klij}$; but $\mathbf{a}$ does not necessarily satisfy the minor symmetries. In the same manner, ψ depends on both the symmetric and skew parts of $\mathbf{e}$. In terms of stress, this implies that the skew part $\sigma_{ij} - \sigma_{ji}$ does not necessarily vanish. As a matter of fact, Cauchy's second law of motion expresses a local version of the balance of angular momentum that reads

$$c_i = \varepsilon_{ijk} \sigma_{jk} \tag{3}$$

where $\mathbf{c}$ is body torque and ε_{ijk} is the permutation symbol. Thus, the solid being polar is equivalent to there being a body torque density linearly dependent over the displacement gradient:

$$c_i = \varepsilon_{ijk} a_{jklm} e_{lm}. \tag{4}$$

Hereafter, in 3D then in 2D, we determine a general expression for isotropic majorly symmetric fourth-order elasticity tensors $\mathbf{a}$, count the maximum number of independent elastic constants they can exhibit and describe the zero modes they possibly support.

2.2. Dimension three

We begin by recalling that the space of second-order tensors can be decomposed into a sum of three subspaces all stable under rotations. Thus, such a decomposition is well suited for the description of an isotropic behavior. These subspaces are those of spherical tensors, symmetric deviatoric tensors and skew tensors. For the displacement gradient $\mathbf{e}$, we write

$$\mathbf{e} = \frac{t}{3}\mathbf{I} + \mathbf{W} + \tilde{\mathbf{e}} \tag{5}$$

where

$$t = \mathrm{tr}\mathbf{e}, \quad \mathbf{W} = \frac{\mathbf{e} - \mathbf{e}^T}{2} \quad \text{and} \quad \tilde{\mathbf{e}} = \frac{\mathbf{e} + \mathbf{e}^T}{2} - \frac{\mathrm{tr}\mathbf{e}}{3}\mathbf{I} \tag{6}$$

are the relative infinitesimal change in volume, the infinitesimal rotation and the deviatoric strain, respectively. Note that the infinitesimal rotation $\mathbf{W}$, being skew, can be represented by a (pseudo)vector $\mathbf{w} = \theta \hat{\mathbf{w}}$ product of the infinitesimal rotation angle θ by the unitary axis of rotation $\hat{\mathbf{w}}$. Component-wise, that vector is

$$w_i = -\frac{1}{2}\varepsilon_{ijk} W_{jk} = -\frac{1}{2}\varepsilon_{ijk} e_{jk}. \tag{7}$$

Accordingly, the deformation energy is a quadratic form

$$\psi(\mathbf{e}) = \psi(t, \mathbf{w}, \tilde{\mathbf{e}}). \tag{8}$$

Given that the behavior is isotropic, the six coupling tensors

$$\frac{\partial^2 \psi}{\partial t^2}, \quad \frac{\partial^2 \psi}{\partial \mathbf{w} \partial \mathbf{w}}, \quad \frac{\partial^2 \psi}{\partial \tilde{\mathbf{e}} \partial \tilde{\mathbf{e}}}, \quad \frac{\partial^2 \psi}{\partial t \partial \mathbf{w}}, \quad \frac{\partial^2 \psi}{\partial \mathbf{w} \partial \tilde{\mathbf{e}}} \quad \text{and} \quad \frac{\partial^2 \psi}{\partial \tilde{\mathbf{e}} \partial t} \tag{9}$$

should all be isotropic.

- The first tensor of the list above is a scalar and is automatically isotropic; it will be denoted κ.
- The second is a second-order tensor; being isotropic, it is proportional to the identity through a modulus denoted α.
- The third is an isotropic majorly symmetric fourth-order tensor $2\boldsymbol{\mu}$ coupling $\tilde{\mathbf{e}}$ to itself. Deviatoric strains being symmetric and traceless, tensor $2\boldsymbol{\mu}$ can further be supposed to satisfy $\mu_{ijkl} = \mu_{jikl}$ and $\mu_{ijkk} = 0$ without loss of generality. Therefore, it is deduced (e.g., from the classical result (44)) that $2\boldsymbol{\mu}$ is proportional to the fourth-order identity through a modulus denoted 2μ.
- The fourth coupling tensor is an isotropic vector and therefore vanishes.
- The fifth is an isotropic third-order tensor and therefore is proportional to the permutation symbol. As it couples $\mathbf{w}$ to $\tilde{\mathbf{e}}$ which is symmetric, it can be set to zero without loss of generality.

- The sixth is an isotropic second-order tensor and therefore is proportional to the identity. As it couples t to $\tilde{\mathbf{e}}$ which is traceless, it can be set to zero without loss of generality as well.

All in all, the elastic energy stored for a deformation $\mathbf{e}$ specifies into

$$\psi = \mu\tilde{\mathbf{e}} : \tilde{\mathbf{e}} + \frac{1}{2}\kappa t^2 + \frac{1}{2}\alpha\theta^2 \tag{10}$$

and features three independent elastic moduli. Once more, Hooke's law is obtained by differentiation of ψ with respect to $\mathbf{e}$; it reads

$$\boldsymbol{\sigma} = 2\mu\tilde{\mathbf{e}} + \kappa t\mathbf{I} + \frac{\alpha}{2}\mathbf{W} \tag{11}$$

and breaks into three parts

$$\tilde{\boldsymbol{\sigma}} = 2\mu\tilde{\mathbf{e}}, \quad p = -\kappa t \quad \text{and} \quad \mathbf{c} = -\alpha\mathbf{w} \tag{12}$$

where

$$\tilde{\boldsymbol{\sigma}} = \frac{\boldsymbol{\sigma} + \boldsymbol{\sigma}^T}{2} + p\mathbf{I}, \quad p = -\frac{\mathrm{tr}\boldsymbol{\sigma}}{3} \quad \text{and} \quad c_i = \varepsilon_{ijk}\sigma_{jk} \tag{13}$$

are deviatoric stress, hydrostatic pressure and body torque, respectively.

Equivalently, the elasticity tensor admits the expression

$$a_{ijkl} = \mu(\delta_{ik}\delta_{jl} + \delta_{il}\delta_{jk}) + \left(\kappa - \frac{2}{3}\mu\right)\delta_{ij}\delta_{kl} + \frac{\alpha}{4}(\delta_{ik}\delta_{jl} - \delta_{il}\delta_{jk}). \tag{14}$$

Therein, the existence of parameter α is characteristic of a polar solid. For $\alpha = 0$, $\mathbf{a}$ is minorly symmetric and the stress tensor is systematically symmetric: we say that the solid is a Cauchy's solid. For $\alpha \neq 0$, $\mathbf{a}$ lacks the minor symmetries and can yield asymmetric stresses: we say that the solid is polar. In the latter case, the skew part of stress directly quantifies the externally applied body torque $\mathbf{c}$ as proportional to the infinitesimal rotation vector $\mathbf{w}$. Therefore, α can be interpreted as a torsional rigidity. As for moduli κ and μ, they express the usual relationships between pressure and change in volume and between shear strains and shear stresses; they are bulk and shear moduli, respectively.

Last, from Eq. (10), it is seen that all three moduli, μ, κ and α, must be positive in order to enforce stability; if either vanishes, the polar solid becomes degenerate in the sense that it exhibits nonzero displacement gradients $\mathbf{e}$ with zero stress $\boldsymbol{\sigma}$. Such gradients are called zero modes and are denoted $\mathbf{e}_{zm}$. For instance, $\mu = 0$ enables five zero modes given by simple shears; $\kappa = 0$ enables a single zero mode, namely a pure dilatation; and $\alpha = 0$ enables three zero modes corresponding to infinitesimal rotations. The latter describes the standard case of a Cauchy's solid. Last, when multiple moduli vanish simultaneously, the foregoing cases can be linearly combined.

2.3. Dimension two

Interestingly, in 2D, isotropy tolerates an extra material parameter denoted β. As a matter of fact, in 2D, the skew part of $\mathbf{e}$ can be represented as a scalar θ. This enables a fourth material parameter coupling θ to t. Therefore, the deformation energy specifies into

$$\psi = \mu\tilde{\mathbf{e}} : \tilde{\mathbf{e}} + \frac{1}{2}\kappa t^2 + \frac{1}{2}\alpha\theta^2 + \beta t\theta \tag{15}$$

and the elasticity tensor into

$$a_{ijkl} = \mu(\delta_{ik}\delta_{jl} + \delta_{il}\delta_{jk}) + (\kappa - \mu)\delta_{ij}\delta_{kl} + \frac{\alpha}{4}J_{ij}J_{kl} + \frac{\beta}{2}(\delta_{ij}J_{kl} + J_{ij}\delta_{kl}). \tag{16}$$

Equivalently, Hooke's law becomes

$$\boldsymbol{\sigma} = (\kappa t + \beta\theta)\mathbf{I} + 2\mu\tilde{\mathbf{e}} + \frac{\beta t + \alpha\theta}{2}\mathbf{J}, \tag{17}$$

where $\mathbf{J}$ is the $\pi/2$ plane rotation. Most notably, hydrostatic pressure and body torque are coupled according to the constitutive relations

$$p = -\kappa t - \beta\theta \quad \text{and} \quad c = -\beta t - \alpha\theta \tag{18}$$

where c and θ are now given by

$$c = -\mathbf{J} : \boldsymbol{\sigma} \quad \text{and} \quad \theta = \frac{1}{2}\mathbf{J} : \mathbf{e}. \tag{19}$$

In order to enforce stability, μ, κ and α should remain positive while the newly found coupling should remain small, or

$$\beta^2 \leq \kappa\alpha, \tag{20}$$

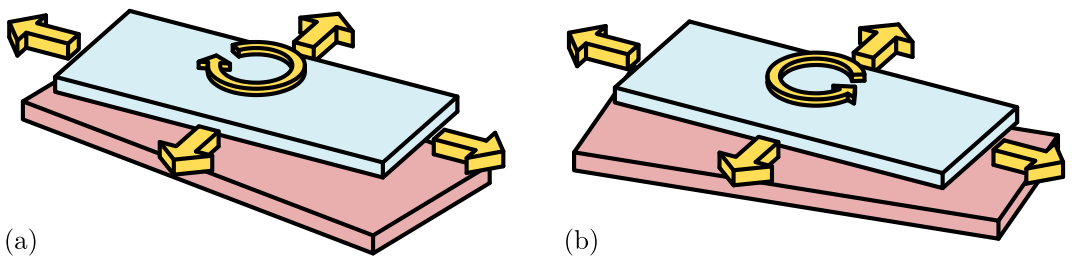

Fig. 1. A sketch of the chiral coupling between infinitesimal rotation and change in area in (a) ambidextral and (b) dextral polar media: top and bottom correspond to reference and current configurations respectively. The arrows illustrate motion, not efforts.

more precisely. Accordingly, in addition to the cases previously discussed in 3D, isotropic polar solids in 2D can also become degenerate if

$$\beta^2 = \kappa\alpha, \tag{21}$$

without μ, κ or α being zero. In that case, the solid admits a unique zero mode $\mathbf{e}_{zm}$ characterized by

$$\tilde{\mathbf{e}}_{zm} = \mathbf{0}, \quad \kappa t + \beta\theta = 0 \quad \text{and} \quad \beta t + \alpha\theta = 0. \tag{22}$$

Consequently, $\mathbf{e}_{zm}$ has only spherical and skew parts and admits the expression $\mathbf{e}_{zm} = a\mathbf{I} + b\mathbf{J}$. Substituting into (22), we find

$$\mathbf{e}_{zm} = \beta\mathbf{I} + 2\kappa\mathbf{J}. \tag{23}$$

Remarkably, 2D isotropic polar solids turn out to be able to support zero modes that are function of their constitutive parameters (e.g., β and κ). As a result, a gradient of polar materials can support a gradient of zero modes. By contrast, in 3D, all supported zero modes are parameter-independent and therefore cannot be continuously varied over space.

2.4. Chirality

Recall that elasticity, being described by an even-order tensor, is automatically inversion-invariant. In 3D, inversion is a reflection meaning that 3D elasticity is automatically nonchiral. In 2D, inversion is not a reflection implying that 2D elasticity can be chiral in principle. Minor symmetry however, combined with isotropy (or any nontrivial symmetry for that matter, see He and Zheng, 1996), does preclude chirality. By contrast, polar solids, as they lack minor symmetry, can be chiral while remaining isotropic. Here, we highlight chirality-related effects in their simplest static manifestation.

For that purpose, consider the uniform deformation of a 2D isotropic polar solid under a purely hydrostatic stress of pressure p, i.e., with $c = 0$. A relationship between the relative infinitesimal change in area t and the infinitesimal rotation θ can be found and reads

$$\theta = -\frac{\beta}{\alpha}t. \tag{24}$$

Accordingly, an increase in area ($t > 0$) is accompanied by a counterclockwise rotation if $\beta < 0$, by a clockwise rotation if $\beta > 0$, and by no rotation if $\beta = 0$, all in the absence of body torque. Thus, isotropic polar solids are chiral when $\beta \neq 0$ and, in that case, are of two types: solids with $\beta < 0$ will be referred to as "dextral" whereas solids with $\beta > 0$ will be referred to as "ambidextral"; see Fig. 1.

A similar conclusion holds when the solid deforms uniformly under a net torque with zero hydrostatic pressure. Note however that the value of the coupling between rotation and change in area is now different in general since $p = 0$ implies

$$\theta = -\frac{\kappa}{\beta}t. \tag{25}$$

Finally, in the critical regime of a degenerate solid, $p = 0$ and $c = 0$ occur simultaneously so that the solid deforms freely under no external efforts. In that case, as the solid changes its area, it rotates either clockwise or anticlockwise depending on its handedness while under zero stress. This stretch-and-rotate motion describes then the zero mode $\mathbf{e}_{zm}$ calculated previously in Eq. (23).

2.5. Propagation of plane harmonic waves

We pursue here our investigation of 2D isotropic polar solids with emphasis on chiral effects but in the dynamic regime this time. The results obtained here for the most part can be readily generalized, or rather adapted, to 3D by setting $\beta = 0$.

Having cloaking applications, as well as related wave phenomena in mind, it is of interest to inspect how harmonic plane waves propagate through polar solids. We let

$$\mathbf{u} = \mathbf{u}_o e^{i(\mathbf{k}\cdot\mathbf{x}-\omega t)} \tag{26}$$

be a candidate solution of the motion equation of wavenumber $\mathbf{k}$ and angular frequency ω. The corresponding eigenvalue problem can then be put in the form

$$\boldsymbol{\Gamma}\mathbf{u}_o = \frac{\omega^2}{k^2}\mathbf{u}_o, \quad [\boldsymbol{\Gamma}] = \frac{1}{\rho}\begin{bmatrix} \mu+\kappa & \beta/2 \\ \beta/2 & \mu+\alpha/4 \end{bmatrix}, \tag{27}$$

where tensor $\boldsymbol{\Gamma}$ has been decomposed in the canonical basis ($\mathbf{k}$, $\mathbf{Jk}$). Matrix $[\boldsymbol{\Gamma}]$ being nondiagonal signifies that, for $\beta \neq 0$, purely longitudinal and purely transverse modes do not exist. This is another symptom of chirality. Indeed, it is expected that the coupling between dilation and rotation precludes purely longitudinal modes and, then necessarily, purely transverse ones as well. The supported modes still have mutually orthogonal polarizations denoted $\mathbf{u}_\pm$ and admitting the expressions

$$[\mathbf{u}_+] = \begin{bmatrix} \cos\gamma \\ -\sin\gamma \end{bmatrix} \quad \text{and} \quad [\mathbf{u}_-] = \begin{bmatrix} \sin\gamma \\ \cos\gamma \end{bmatrix}, \quad -\pi/2 < \gamma \leq \pi/2. \tag{28}$$

The corresponding eigenvalues are then

$$c_\pm^2 = \frac{\mu}{\rho} + \frac{1}{2\rho}(\kappa+\alpha/4) \pm \frac{1}{2\rho}\sqrt{(\kappa-\alpha/4)^2+\beta^2} \tag{29}$$

and are equal to the propagation velocities $c_\pm$ squared of the respective modes. It will also be useful to introduce the centered normalized wave velocities

$$\bar{c}_\pm = \sqrt{\frac{\rho c_\pm^2 - \mu}{\kappa+\alpha/4}}. \tag{30}$$

As for angle γ, it is characterized by

$$\cos(2\gamma) = \frac{\kappa-\alpha/4}{\sqrt{(\kappa-\alpha/4)^2+\beta^2}} \quad \text{and} \quad \sin(2\gamma) = -\frac{\beta}{\sqrt{(\kappa-\alpha/4)^2+\beta^2}}. \tag{31}$$

The range of possible polarizations is illustrated on Fig. 2. Therein, the x-axis corresponds to parameter $(\kappa-\alpha/4)/(\kappa+\alpha/4)$ and qualitatively measures to which degree stress symmetry is broken, i.e., how far the medium is from a Cauchy's medium (point C). As for the y-axis, it corresponds to parameter $\beta/(\kappa+\alpha/4)$ and measures the amplitude and handedness of chiral effects. Enforcing stability implies that only pairs of parameters falling within the big circle of equation $\beta^2 = \kappa\alpha$ are within reach. For each pair of parameters, a cross represents the orthogonal polarizations of the $\mathbf{u}_+$ and $\mathbf{u}_-$ modes oriented with respect to wavenumber $\mathbf{k}$ supposed everywhere horizontal and pointing towards the right. The length of the longer mark is proportional to $\bar{c}_+$, that of the shorter one to $\bar{c}_-$. Thus, starting at point C and going deeper into quadrant (I), the faster mode $\mathbf{u}_+$ (resp., the slower mode $\mathbf{u}_-$) becomes less and less longitudinal (resp., transverse). As we reach the y-axis, modes $\mathbf{u}_\pm$ are at $\pm\pi/4$ from $\mathbf{k}$. As we go deeper into the second quadrant, the faster (resp., slower) mode becomes more and more transverse (resp., longitudinal). As we reach the other side of the x-axis, i.e., $\kappa < \alpha/4$ and $\beta = 0$, the faster (resp., slower) mode becomes purely transverse (resp., longitudinal). Last, at the origin, $\beta = 0$, $\kappa = \alpha/4$, all polarizations are possible, a fact symbolized on the plot with a small circle. In that case, all modes propagate at the same centered normalized velocity $\bar{c}_\pm = 1/\sqrt{2}$.

2.6. Example: Grounded hexachiral lattices

Isotropic degenerate polar solids, their mechanics and the potentially useful phenomena they host, all remain a theoretical exercise so long as we have not demonstrated that they can actually be designed. It is the purpose of this subsection to provide designs of lattice materials whose behavior in the homogenization limit is that of an isotropic degenerate polar solid. Aiming for a chiral yet isotropic outcome, the hexachiral spring-mass lattice of Fig. 3a emerges as a natural candidate (see also Bacigalupo and Gambarotta, 2014; Liu et al., 2012; Rosi and Auffray, 2016; Spadoni and Ruzzene, 2012; Spadoni et al., 2009). Its unit cell contains a single mass of value m and radius b and three springs of constant k and directions $\mathbf{n}_i$ that are tangent to the masses' outer circumferences. Last, call $\mathbf{r}_j$ the three elementary lattice vectors and call γ the (oriented) angle between $\mathbf{n}_i$ and $\mathbf{r}_i$.

Loosely speaking, a polar solid is one that resists rotations. Polar solids are therefore necessarily grounded. Unlike common elastic foundations that resist displacements, polar solids require a foundation that resists displacement gradients, e.g., rotations, without hindering the displacements themselves. Thus, we connect each mass to a parallel rigid plane through a torsional spring of constant $\eta = 12bb'k$ where b' is a positive radius equivalent to a torsional rigidity; see Fig. 3b. The spring being vertical, small inplane displacements of the masses remain unaware of the ground. In contrast, mass rotation is penalized by a restoring torque $-\eta\phi$ proportional to the rotation angle ϕ.

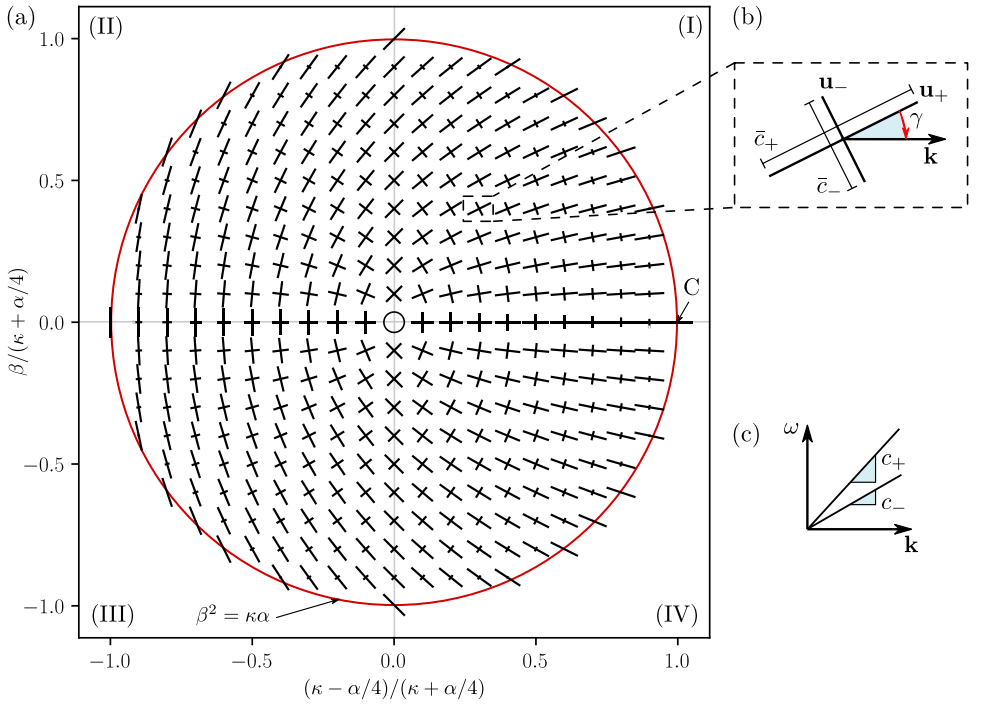

Fig. 2. Plane harmonic waves in a polar isotropic solid. (a) Polarization field in the $((\kappa-\alpha/4)/(\kappa+\alpha/4), \beta/(\kappa-\alpha/4))$-space: the big circle bounds the stable region $\beta^2 \le \kappa\alpha$; point C corresponds to a Cauchy's medium. (b) Magnified view: at each pair of parameters, a cross represents the orthogonal polarizations of the $\mathbf{u}_+$ and $\mathbf{u}_-$ modes; the lengths of the marks are proportional to the normalized wave velocities $\bar{c}_\pm$. (c) A typical dispersion curve.

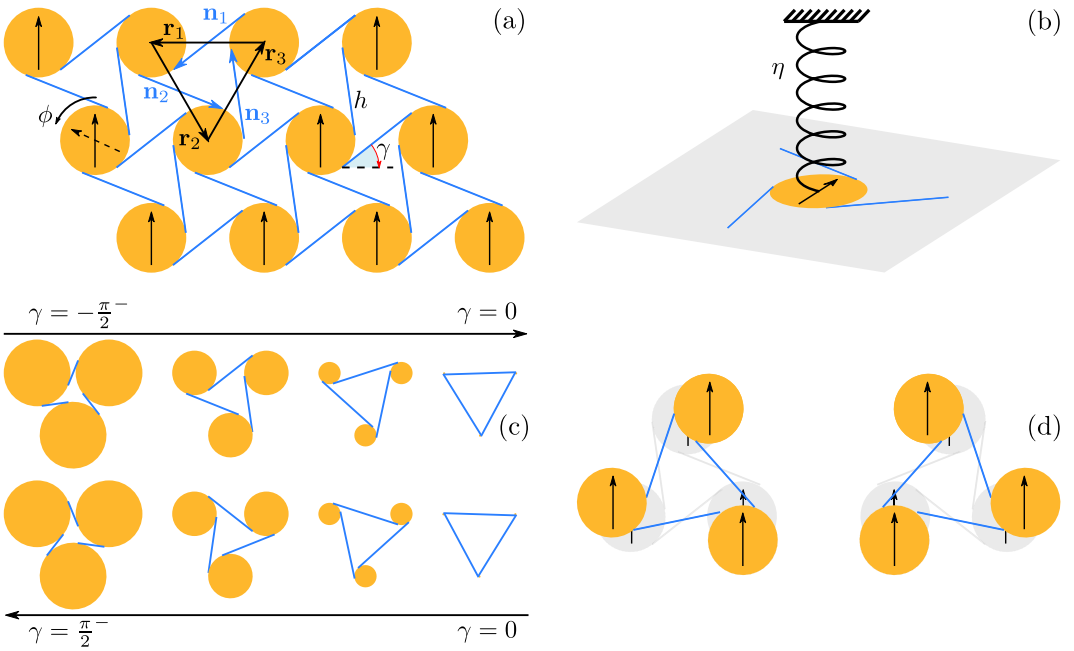

Fig. 3. Grounded hexachiral lattices as isotropic polar solids. (a) An annotated example with $\gamma < 0$; the arrows serve as a reference to the masses' initial orientation. (b) Grounding mechanism: An out-of-plane torsional spring is attached to each mass thus providing a restoring torque acting against mass rotation without hindering displacements. (c) Unit cell variations parametrized with $\gamma \in (-\pi/2, \pi/2)$. (d) The action of the zero mode on the configuration of a unit cell for an ambidextral (left) and a dextral (right) solid: reference state is in the background, the deformed one in the foreground.

Hence, the elastic energy of the lattice per unit cell area a for a displacement gradient $\mathbf{e}$ is given by

$$\psi(\mathbf{e}) = \min_{\phi} E(\mathbf{e}, \phi) \quad \text{with} \quad E(\mathbf{e}, \phi) = \frac{k}{2a} \sum_i (\langle \mathbf{e}\mathbf{r}_i, \mathbf{n}_i \rangle - 2b\phi)^2 + \frac{\eta}{2a}\phi^2. \tag{32}$$

At the minimum, the rotation angle satisfies the zero derivative condition

$$\frac{\partial E}{\partial \phi} = 0, \quad \text{i.e.,} \quad -2bk \sum_i (\langle \mathbf{e}\mathbf{r}_i, \mathbf{n}_i \rangle - 2b\phi) + \eta\phi = 0, \tag{33}$$

and is given by

$$\phi = \mathbf{s} : \mathbf{e} \quad \text{where} \quad \mathbf{s} = \frac{1}{6(b+b')} \sum_i \mathbf{n}_i \otimes \mathbf{r}_i = \frac{r}{4(b+b')} \mathbf{R}^T \tag{34}$$

and $\mathbf{R}$ is the plane rotation of angle γ. Consequently, the elastic energy density can be recast into

$$\psi(\mathbf{e}) = \frac{k}{2a} \sum_i (\langle \mathbf{e}\mathbf{r}_i, \mathbf{n}_i \rangle - 2b\mathbf{s} : \mathbf{e})^2 + \frac{\eta}{2a} (\mathbf{s} : \mathbf{e})^2. \tag{35}$$

Thus, the elasticity tensor of the lattice is

$$\mathbf{a} = \frac{\partial^2 \psi}{\partial \mathbf{e} \partial \mathbf{e}} = \frac{k}{a} \sum_i (\mathbf{n}_i \otimes \mathbf{r}_i - 2b\mathbf{s}) \otimes (\mathbf{n}_i \otimes \mathbf{r}_i - 2b\mathbf{s}) + \frac{\eta}{a} \mathbf{s} \otimes \mathbf{s}, \tag{36}$$

and, skipping a few index manipulations, can be expressed by

$$a_{pqrs} = \frac{k\sqrt{3}}{4} \left(\frac{b' - b}{b' + b} R_{qp} R_{sr} + R_{sp} R_{qr} + \delta_{pr} \delta_{qs} \right). \tag{37}$$

Therefrom, $\mathbf{a}$ can be readily verified to be isotropic and the material parameters of the effective polar solid can be extracted. They read

$$\mu = \frac{k\sqrt{3}}{4}, \qquad \kappa = \frac{kb'\sqrt{3}}{2(b+b')} \cos^2\gamma, \qquad \alpha = \frac{2kb'\sqrt{3}}{b+b'} \sin^2\gamma \qquad \text{and} \qquad \beta = -\frac{kb'\sqrt{3}}{b+b'} \cos\gamma \sin\gamma. \tag{38}$$

In particular, relation (21) holds systematically meaning that the effective polar solid is degenerate. The corresponding zero mode has been illustrated on Fig. 3d.

Formulae (38) are perhaps more useful inverted so as to yield the lattice parameters necessary for targeting the elastic parameters of a given degenerate isotropic polar solid. We find

$$k = \frac{4\mu}{\sqrt{3}}, \quad \frac{b'}{b} = \frac{\kappa + \frac{\alpha}{4}}{2\mu - \kappa - \frac{\alpha}{4}} \quad \text{and} \quad \gamma = \text{sgn}\beta \arctan \sqrt{\frac{\alpha/4}{\kappa}}. \tag{39}$$

Add to that the expression of the mass density of the masses given by

$$\frac{m}{\pi b^2} = \frac{2\sqrt{3}\rho}{\pi} \left(1 + \frac{\kappa}{\alpha/4} \right), \tag{40}$$

where ρ is the mass density of the target solid.

It is noteworthy that the proposed lattices remain stable in the homogenization limit even when b', or equivalently η, is negative as long as $1 + b/b'$ is positive. If however the stability of the lattice's constitutive elements, taken separately, is desired as well, then b' must be positive. In conclusion, under the element-wise stability requirement, the proposed grounded hexachiral lattices can target all degenerate isotropic polar solids satisfying

$$2\mu \geq \kappa + \frac{\alpha}{4}. \tag{41}$$

The salient static and dynamic characteristics of these lattices, in the homogenization limit, can of course be deduced from the general study of the previous subsections. More importantly, in any application (e.g., cloaking) where such polar solids are needed, the suggested lattices can be used but only so in a sufficiently low frequency regime.

3. Conformal transformation theory

In this section, we briefly recall the general transformation method and then specify it to conformal transformations. We prove that conformal transformations map a 2D isotropic elastic solid into a gradient of isotropic degenerate polar materials. This is done by exhibiting the transformation rules that relate the original and image constitutive tensors. It should be noted that 3D conformal transformations are limited to translations, rotations, reflections, scalings and inversions. By contrast, in 2D, all analytic functions of a complex variable are conformal. This implies that the use of conformal transformations for field manipulation purposes while avoiding anisotropic constitutive materials is far more potent in 2D than in 3D. Thus, from now on, we restrict our presentation to 2D.

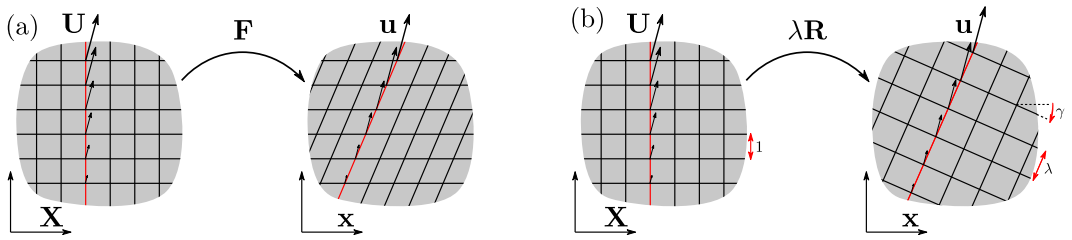

Fig. 4. Local view of the transformation method: (a) nonconformal; (b) conformal. Note how displacements are redistributed but otherwise remain the same. This fictitious redistribution can be realized by enforcing the rules (42).

3.1. General transformation rules

Let $\mathbf{U}$ be the displacement field over a body $\{\mathbf{X}\}$ of mass density R and elasticity tensor $\mathbf{A}$. It is of interest to determine what fields ρ and $\mathbf{a}$ should replace R and $\mathbf{A}$ so as to redistribute the displacements $\mathbf{U}$ in a controlled and purposeful manner. Facing that inverse problem, the transformation method provides a solution. Specifically, letting $\mathbf{x} = \boldsymbol{\phi}(\mathbf{X})$ transform $\{\mathbf{X}\}$ into a new body $\{\mathbf{x}\}$, the field $\mathbf{u}(\mathbf{x}) = \mathbf{U}(\mathbf{X})$ reigns over $\{\mathbf{x}\}$ if the new properties derive from the original ones following

$$\rho = R/J \quad \text{and} \quad a_{ijkl} = F_{jp}F_{lq}A_{ipkq}/J, \tag{42}$$

with $F_{ij} = \partial x_i/\partial X_j$ and $J = \det \mathbf{F}$ (Norris and Shuvalov, 2011); see Fig. 4. The Hooke's law corresponding to the new moduli a_{ijkl} then reads

$$\sigma_{ij} = a_{ijkl}e_{kl} = F_{jp}F_{lq}A_{ipkq}e_{kl}/J, \tag{43}$$

where $e_{kl} = \partial u_k/\partial x_l$ is the displacement gradient.

Note that we have set $\mathbf{u}(\mathbf{x}) = \mathbf{U}(\mathbf{X})$ whereby the point of application of a displacement changes but not the displacement itself. This transformation rule was first introduced by Brun et al. (2009) and is adopted here as it is capable of preserving isotropy. Other gauges, with $\mathbf{u}(\mathbf{x}) \neq \mathbf{U}(\mathbf{X})$, were suggested by Milton et al. (2006) and by Norris and Shuvalov (2011); these do not seem to preserve isotropy except in trivial cases.

3.2. Conformal transformation rules

Suppose now that $\mathbf{A}$ satisfies the major and minor index symmetries (i.e., $A_{ijkl} = A_{klij} = A_{jikl}$) and is isotropic with a shear modulus μ_o and a bulk modulus κ_o, namely

$$A_{ijkl} = \mu_o(\delta_{ik}\delta_{jl} + \delta_{il}\delta_{jk}) + (\kappa_o - \mu_o)\delta_{ij}\delta_{kl}. \tag{44}$$

Also, let $\boldsymbol{\phi}$ be conformal in the sense that it preserves oriented angles. Therefore, $\mathbf{F}$ is shear-free and reads as the product of a pure dilatation by a plane rotation, i.e.,

$$\mathbf{F} = \lambda\mathbf{R} \tag{45}$$

where $\lambda = \sqrt{J}$ is a positive stretch ratio and $\mathbf{R}$ is again the plane rotation of angle γ.

Employing the transformation rule (42), and skipping elementary index manipulations, we deduce that $\mathbf{a}$ takes the form (16) with the elasticity constants μ, κ, α and β given respectively by

$$\mu = \mu_o, \quad \kappa = \kappa_o \cos^2\gamma, \quad \alpha = 4\kappa_o \sin^2\gamma \quad \text{and} \quad \beta = -2\kappa_o \cos\gamma \sin\gamma. \tag{46}$$

In particular, (*i*) the shear modulus is invariant; (*ii*) the local stretch λ is irrelevant; and (*iii*) the image parameters systematically satisfy

$$\alpha\kappa = 4\kappa_o^2 \cos^2\gamma \sin^2\gamma = \beta^2. \tag{47}$$

In conclusion, in 2D, we have proven that conformal transformations applied to an isotropic solid yield a gradient of isotropic denegerate polar materials.

3.3. Discussion

As described earlier, a conformal transformation locally resembles a rotation of angle γ followed by a dilatation of ratio λ. Thus, a plane harmonic wave traveling along a direction inclined at an angle δ away from an absolute axis in body $\{\mathbf{X}\}$ has an image that travels at angle $\delta + \gamma$ away from the same axis in $\{\mathbf{x}\}$. Given the gauge $\mathbf{u}(\mathbf{x}) = \mathbf{U}(\mathbf{X})$, the wave and its image have identical amplitudes. Accordingly, if the wave is longitudinally polarized in $\{\mathbf{X}\}$, then its image is polarized at angle $-\gamma$ with respect to the propagation direction in $\{\mathbf{x}\}$; similarly, if it is transversally polarized in $\{\mathbf{X}\}$, then its image is polarized at an angle $\pi/2 - \gamma$; see Fig. 4b.

Furthermore, since space in $\{\mathbf{x}\}$ is stretched by a ratio λ in comparison to $\{\mathbf{X}\}$, the image of a wave is expected to travel at lower (resp., higher) speed if $\lambda < 1$ (resp., $\lambda > 1$). Equivalently, the transformation rule for mass density,

$$\rho = R/\lambda^2, \tag{48}$$

implies the same decrease or increase in propagation speeds. By that logic, it is expected that pressure and shear waves have images that all propagate at the same speeds

$$c_+ = \lambda\sqrt{\frac{\kappa_o + \mu_o}{R}} \quad \text{and} \quad c_- = \lambda\sqrt{\frac{\mu_o}{R}}, \tag{49}$$

respectively.

Note that these effects, namely bias in polarization and change in speed, can be quantitatively checked by injecting the derived expressions (46) into the formulae (29). Both derivations (and notations) are therefore consistent.

4. Application: Conformal carpet cloaking

Cloaking is a notable application of the general transformation method. Here, using strictly conformal transformations, we demonstrate a version of cloaking known as "carpet" cloaking by hiding an inclusion along the free boundary of an elastic half-plane. The geometry and elastic parameters of the cloak as well as of its lattice microstructure are derived and numerical simulations are carried so as to assess cloaking performance.

4.1. Geometry

Let $\{\mathbf{x}\}$ be an elastic half-space composed of three regions: the first is a void half-disk of radius a; the second is a coating of that void of approximate width $2w$ and height h; and the third is an isotropic homogeneous background of elastic constants κ_o and μ_o. Let $\boldsymbol{\phi}$ be a transformation whose inverse eclipses the void of radius a while leaving the background invariant; see Fig. 5. Thus, by filling the coating with a gradient of materials following the transformation rules (42), body $\{\mathbf{x}\}$ can be seen as the image of a homogeneous isotropic elastic half-space $\{\mathbf{X}\}$ of parameters κ_o and μ_o. Accordingly, the fields that reign over $\{\mathbf{x}\}$ can be obtained by redistributing the fields that reign over $\{\mathbf{X}\}$. In particular, having assumed $\boldsymbol{\phi}(\mathbf{X}) = \mathbf{X}$ over the background, the fields over there remain unaltered. Consequently, from the perspective of an observer located in the background, bodies $\{\mathbf{x}\}$ and $\{\mathbf{X}\}$ are indistinguishable meaning that the void of radius a has been cloaked.

Unfortunately, when $\boldsymbol{\phi}$ is conformal, $\boldsymbol{\phi}(\mathbf{X}) = \mathbf{X}$ over any region of finite extent readily implies, by the uniqueness of analytic continuation, that $\boldsymbol{\phi}(\mathbf{X}) = \mathbf{X}$ everywhere thus making $\{\mathbf{x}\}$ and $\{\mathbf{X}\}$ identical and leaving no room for a void to be cloaked. To circumvent this limitation, we only enforce $\boldsymbol{\phi}(\mathbf{X}) = \mathbf{X}$ in the limit $|\mathbf{X}| \to \infty$ and take

$$\mathbf{x} = \boldsymbol{\phi}(\mathbf{X}) = \begin{cases} (\mathbf{X} + \sqrt{\mathbf{X}^2 - 4a^2})/2, & \text{for } |\mathbf{X}| \text{ finite}, \\ \mathbf{X}, & \text{for } |\mathbf{X}| \to \infty, \end{cases} \tag{50}$$

where $\mathbf{x}$ and $\mathbf{X}$ are represented by complex numbers and where the complex square root is taken to have a positive imaginary part. Fig. 5 illustrates the action of $\boldsymbol{\phi}$. Therein, it is visible that $\boldsymbol{\phi}$ is conformal since it transforms a square grid into another square grid.

In practice, and in order to bound the cloak's domain, we adopt

$$\mathbf{x} = \boldsymbol{\phi}(\mathbf{X}) = \begin{cases} (\mathbf{X} + \sqrt{\mathbf{X}^2 - 4a^2})/2 & \text{for } \mathbf{X} \in D \equiv (-w, w) + i(0, h), \\ \mathbf{X}, & \text{for } \mathbf{X} \notin D, \end{cases} \tag{51}$$

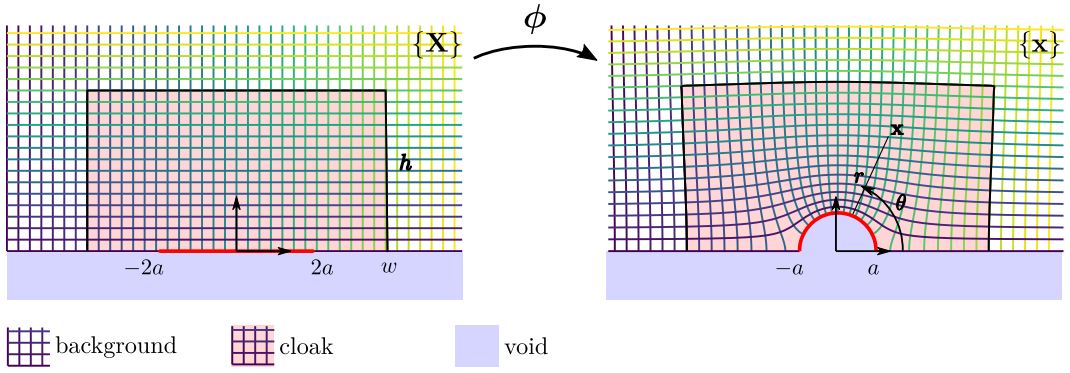

Fig. 5. The contour lines of the Cartesian coordinates of $\mathbf{X}$ before and after transformation. Note that the real segment $[-2a, 2a]$ transforms into a semi circle of radius a thus leaving a void along the free boundary of the half-plane where objects can be hidden. The domain of the cloak is highlighted: originally, it is a rectangle of width $2w$ and height h.

where the image of the rectangle D, i.e., $\boldsymbol{\phi}(D)$, defines the cloak's domain. Accordingly, $\boldsymbol{\phi}$ is piecewise conformal and is discontinuous along the boundary of D; as a consequence, cloaking is expected to be approximate but improves as w and h get larger. Cloaking becomes perfect in the theoretical limit $w, h \to \infty$.

4.2. Elastic parameters

From expression (50), it is possible to derive that, within the cloak,

$$\frac{\partial \mathbf{X}}{\partial \mathbf{x}} = -\frac{a^2}{\mathbf{x}^2} + 1. \tag{52}$$

By extracting real and imaginary parts, the above relation can be recast into the matrix form

$$\mathbf{F}^{-1} = \left(1 - \frac{a^2}{r^2}\cos(2\theta)\right)\mathbf{I} + \frac{a^2}{r^2}\sin(2\theta)\mathbf{J}, \tag{53}$$

with

$$\mathbf{x} = r\exp(i\theta); \tag{54}$$

see Fig. 5. Elementary algebraic manipulations then permit to reveal that $\mathbf{F}$ is the product of a pure dilatation of stretch λ by a plane rotation of angle γ respectively given by

$$\begin{aligned} \lambda &= \frac{1}{\sqrt{a^4/r^4 + 1 - 2a^2/r^2\cos(2\theta)}}, \\ \cos\gamma &= \frac{1 - a^2/r^2\cos(2\theta)}{\sqrt{a^4/r^4 + 1 - 2a^2/r^2\cos(2\theta)}} \\ \text{and} \quad \sin\gamma &= -\frac{a^2/r^2\sin(2\theta)}{\sqrt{a^4/r^4 + 1 - 2a^2/r^2\cos(2\theta)}}. \end{aligned} \tag{55}$$

With these formulae, the elastic parameters and mass density of the cloak can be determined for each position $\mathbf{x}$ by applying the transformation rules (46) and (48).

4.3. Lattice microstructure

To construct a lattice model of the cloak, we determine the way in which the polar hexachiral lattices investigated earlier need to be graded and spatially distributed to fit the local elastic parameters of the cloak. First, we discretize domain D, including its boundary, into a finite hexagonal point lattice with a sufficiently small lattice parameter δ. The points are transformed by $\boldsymbol{\phi}$ and now constitute a discretization of the cloak's domain $\boldsymbol{\phi}(D)$ with a local lattice parameter $\lambda\delta$. Then, at each point, a rigid circular mass is centered and given the radius $\delta\lambda\sin(\gamma)/2$. Last, each mass is grounded using a torsional spring of constant η and each pair of neighboring masses are connected along a common internal tangent using a linear spring of constant k; see Fig. 3 for which tangent to select depending on the sign of angle γ. The various steps of this construction are outlined on Fig. 6.

It is important to highlight that the lattice parameters are $\mathbf{x}$-, or equivalently (r, θ)-, dependent. Specifically, Eqs. (39) and (40) determine the lattice parameters $(k, b'/b, \gamma, b, m)$ in function of the cloak's effective parameters $(\mu, \kappa, \alpha, \beta, \rho)$; Eqs. (46) and (48) provide expressions of $(\mu, \kappa, \alpha, \beta, \rho)$ in function of the background medium constitutive parameters (μ_o, κ_o, R) and of the transformation gradient's parameters (λ, γ); last, Eq. (55) yields (λ, γ) in function of position (r, θ). All in all, the lattice parameters read

$$\begin{aligned} k &= \frac{4\mu_o}{\sqrt{3}}, \\ \frac{b'}{b} &= \frac{\kappa_o}{2\mu_o - \kappa_o}, \\ \gamma &= -\arctan\left(\frac{a^2/r^2\sin(2\theta)}{1 - a^2/r^2\cos(2\theta)}\right), \\ b &= \frac{\delta}{2}\frac{a^2/r^2\sin(2\theta)}{a^4/r^4 + 1 - 2a^2/r^2\cos(2\theta)} \\ \text{and} \quad m &= \frac{\sqrt{3}}{2}R\delta^2. \end{aligned} \tag{56}$$

Hereafter, for simplicity, we consider the case $2\mu_o = \kappa_o$ for which b'/b is infinite meaning that the masses' rotational degree of freedom is completely suppressed.

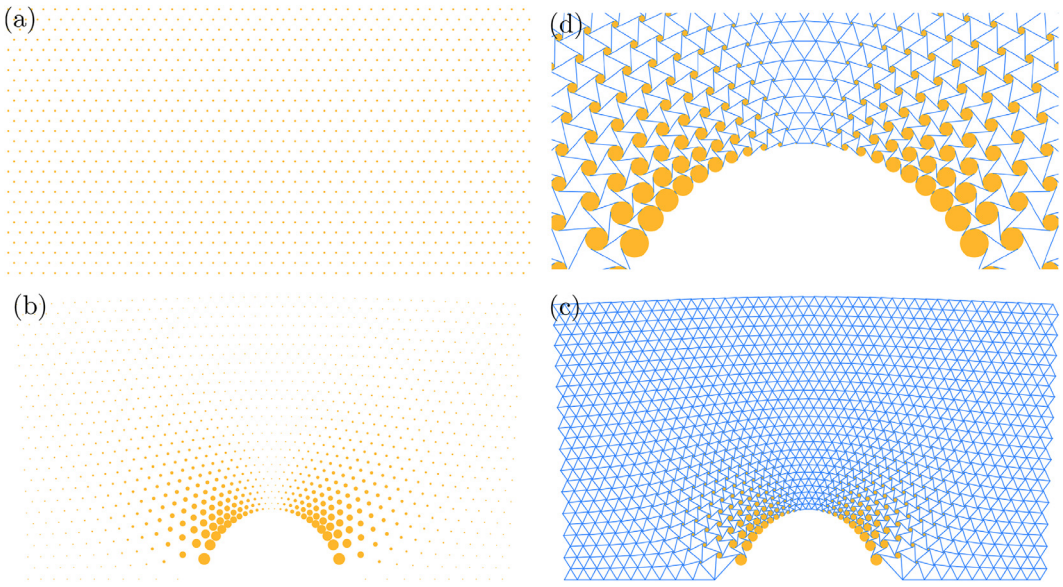

Fig. 6. Building the lattice cloak in three steps: in step (a), the domain D is discretized; in step (b), the points are transformed by $\boldsymbol{\phi}$ into a discretization of the cloak's domain $\boldsymbol{\phi}(D)$; at each point, a mass is centered and grounded; in step (c), masses are connected along common internal tangent lines. On (d) is a magnified view of the cloak's geometry near its vertical axis of symmetry. Notice in particular the change in chirality occurring at the crossing of that axis.

Note that the element-wise stability requirement of Eq. (41) can be recast into a condition weighing on the elastic parameters of the background medium, namely

$$2\mu_o \leq \kappa_o. \tag{57}$$

Consequently, it is only for such background media that the proposed lattice is element-wise stable. For other backgrounds, other lattices are to be found.

4.4. Cloaking simulations

We are now ready to perform cloaking simulations. We set the background medium to a plate made out of an Aluminum-like material with a mass density of 2700 kg/m^3, a shear modulus of 25 GPa, a bulk modulus of 66.67 GPa and a thickness of 1mm. Thus, the 2D plane stress equivalent parameters of the background are given by

$$R = 2.7\,\mathrm{kg/m^2}, \quad \kappa_o = 2\mu_o = 50\mathrm{MPa.m}. \tag{58}$$

The cloak's original dimensions are $2w = 300$ mm by $h = 130$ mm whereas the cloaked void has a radius $a = 40$ mm. The lattice parameter δ was chosen sufficiently small so as to enable satisfactory cloaking performance but not too small so as to avoid impractical simulation times. A good compromise was found at about $\delta = 6.67$ mm for a loading frequency of $f_o = 25$ kHz. Equivalently, the lattice cloak contains 44 to 45 unit cells in its horizontal span and 27 to 28 unit cells in its vertical span. The simulations presented next were carried at f_o; evidently, the cloaking performance is expected to improve for lower frequencies, or eventually in statics. Conversely, the performance is expected to gradually deteriorate for higher frequencies and as the probing wavelength approaches the lattice parameter. Simulations were performed using the finite element method over the continuum background coupled to a weak formulation of Newton's equations over the discrete domain of the cloak.

Simulation results are presented in two series of plots tabulated on Figs. 7 and 8. In all cases, a plane wave with a Gaussian profile is generated by forcing the displacements along a black line visible in the simulation domain. Perfectly matched layers are appended to said domain so as to avoid parasitic reflections. The parameters of the simulation were varied so as to thoroughly characterize the cloak's performance: Figs. 7 and 8 respectively correspond to pressure and shear probing waves. On each Figure, the prefix "p" (resp., "s") identifies the contour plots of the normalized pressure (resp., shear) component whereas the suffixes "0", "30" and "60" correspond, in degrees, to the angle of incidence. The cloaking performance is assessed based on several references: plots in column (a) correspond to the background medium with its free boundary unaltered; in column (b), an uncoated circular void is added; in column (c), the void is coated with a cloak made out of fictitious continuous materials; last, in column (d), the void is coated with the proposed lattice cloak. Accordingly,

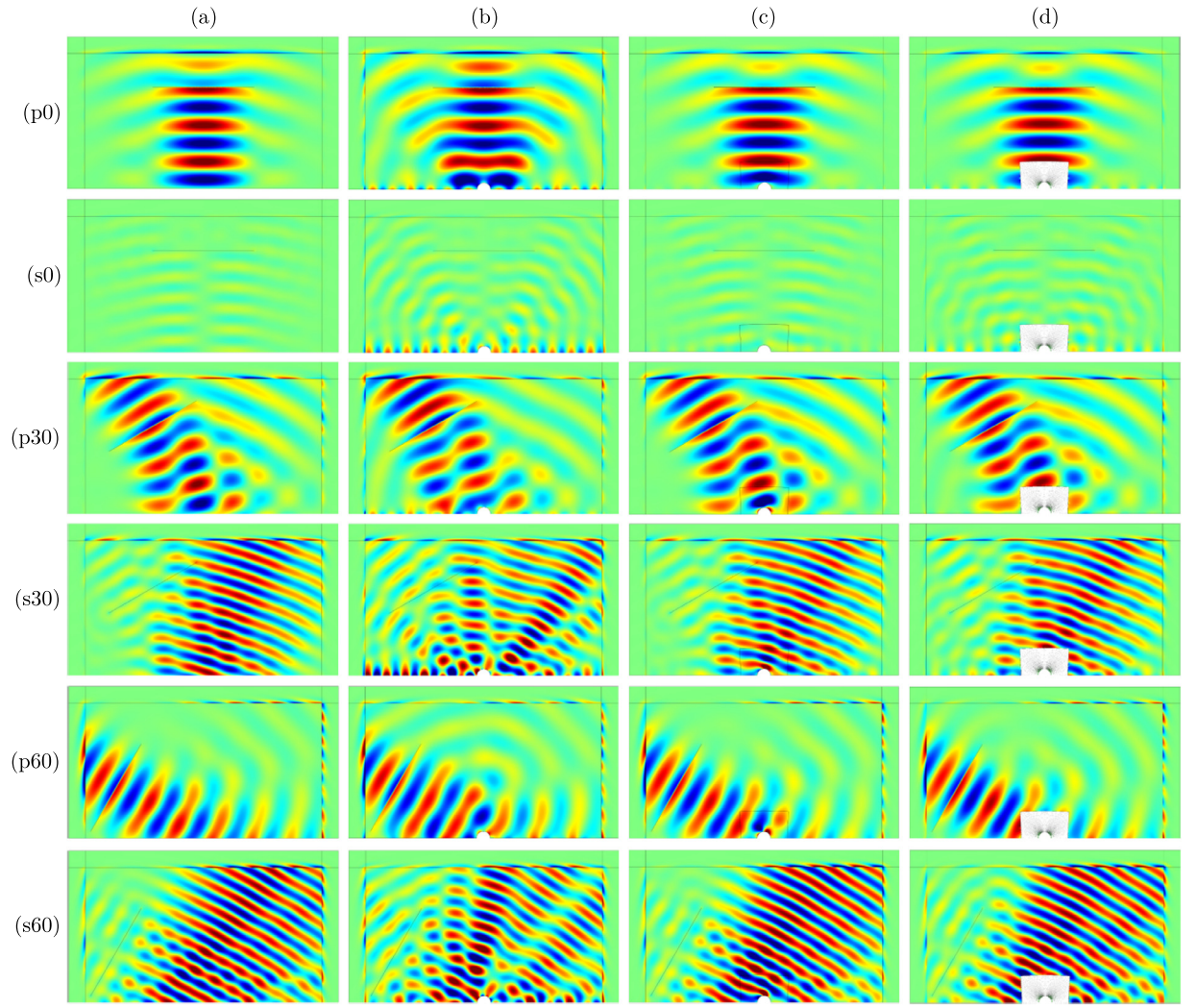

Fig. 7. Normalized contour plots of the pressure and shear components under pressure incidence. Plots' nomenclature: "p" → pressure; "s" → shear; "0", "30" and "60" → the angle of incidence in degrees; (a) → the background medium unaltered; (b) → the background with an uncoated void; (c) → the background with a void cloaked using fictitious continuous materials; (d) → the background with a void cloaked using the proposed lattice.

comparing column (d) to (a) measures the total cloaking error; comparing (d) to (b) measures the amount of scattering suppressed by the lattice cloak; and, comparing (d) to (c) measures a partial cloaking error, the one introduced by the fact that the lattice is not yet operating in the homogenization limit. The remaining cloaking error comes from the fact that the cloak's domain is not infinite and can be visualized by comparing column (c) to (a).

The results demonstrate overall a satisfactory cloaking performance and consistently so over a range of angles of incidence while in the presence of coupled pressure and shear fields. Notably, in addition to suppressing pressure and shear bulk scattering, the lattice cloak is capable of mitigating the generation of surface Rayleigh waves. Consider for instance the case of normal shear incidence of Fig. 8, plots (p0,s0) × (a–d). It is seen that the uncoated void causes a quasi-total conversion of the incident shear wave into a scattered surface Rayleigh wave. The lattice cloak, as well as its theoretical continuous limit, manage however to suppress this scattering and arrange for the incident shear wave to be totally and normally reflected, unconverted.

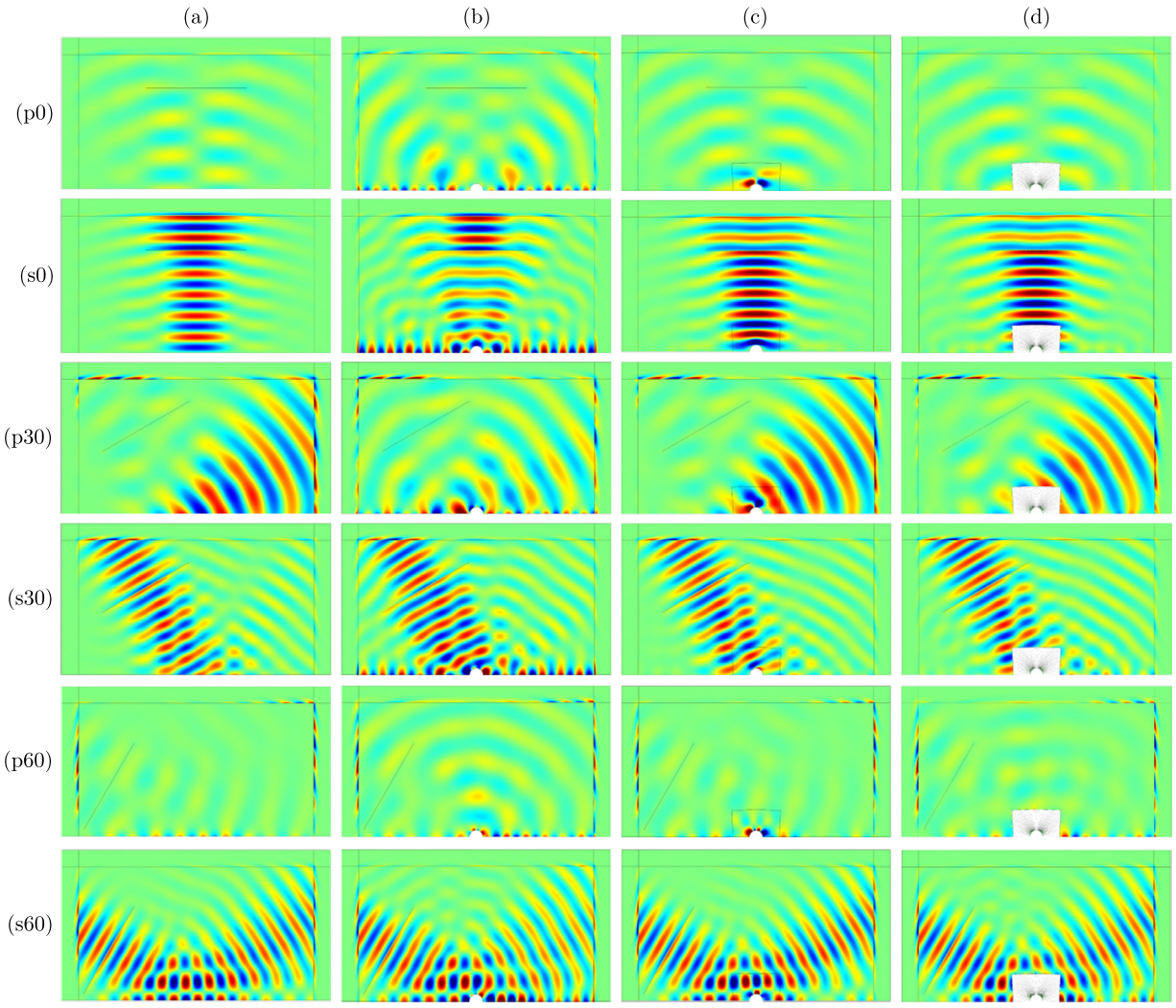

Fig. 8. Normalized contour plots of the pressure and shear components under shear incidence. Plots' nomenclature: "p" → pressure; "s" → shear; "0", "30" and "60" → the angle of incidence in degrees; (a) → the background medium unaltered; (b) → the background with an uncoated void; (c) → the background with a void cloaked using fictitious continuous materials; (d) → the background with a void cloaked using the proposed lattice.

5. Conclusion

As stress symmetry breaks down, additional constitutive parameters emerge and modify Hooke's law. The resulting theory was referred to as polar elasticity. When degenerate, polar elastic solids have been proven to emerge in the context of transformation elasticity where the underlying spatial transformation is conformal. In these cases, rules relating the elastic parameters pre- and post-transformation were derived. As an application, a carpet cloak composed of a gradient of isotropic degenerate polar lattice materials was designed and numerically tested.

The adoption of conformal transformations in the present contribution was motivated by the fact that they preserve isotropy. This raises the question of whether other classes of geometric transformations preserve other classes of material symmetries. Future efforts aimed at such classifications, under different transformation gauges, should be beneficial to the understanding of elastic materials whose behavior is form-invariant and therefore to the design and fabrication of elastic invisibility cloaks and other elastic wave manipulation devices.

Acknowledgement

This work is supported by the Army Research office under Grant No. W911NF-18-1-0031 with Program Manager Dr. David M. Stepp.

References

Auffray, N., Bouchet, R., Bréchet, Y., 2010. Strain gradient elastic homogenization of bidimensional cellular media. Int. J. Solids Struct. 47, 1698–1710.
Bacigalupo, A., Gambarotta, L., 2014. Homogenization of periodic hexa- and tetrachiral cellular solids. Compos. Struct. 116, 461–476.
Brun, M., Colquitt, D.J., Jones, I.S., Movchan, A.B., Movchan, N.V., 2014. Transformation cloaking and radial approximations for flexural waves in elastic plates. New J. Phys. 16, 093020.
Brun, M., Guenneau, S., Movchan, A.B., 2009. Achieving control of in-plane elastic waves. Appl. Phys. Lett. 94, 061903.
Cemal Eringen, A., 1999. Microcontinuum Field Theories I: Foundations and Solids. Springer, New York.
Chen, H., Chan, C.T., 2007. Acoustic cloaking in three dimensions using acoustic metamaterials. Appl. Phys. Lett. 91, 183518.
Chen, Y., Hu, J., Huang, G.L., 2016. A design of active elastic metamaterials for control of flexural waves using the transformation method. J. Intell. Mater. Syst. Struct. 27, 1337–1347.
Chen, Y., Liu, X., Hu, G., 2014. Micropolar modeling of planar orthotropic rectangular chiral lattices. Comptes Rendus - Mec. 342, 273–283.
Colquitt, D.J., Brun, M., Gei, M., Movchan, A.B., Movchan, N.V., Jones, I.S., 2014. Transformation elastodynamics and cloaking for flexural waves. J. Mech. Phys. Solids 72, 131–143.
Cosserat, E., Cosserat, F., 1909. Théorie Des Corps Déformables. Hermann, Paris.
Cummer, S.A., Schurig, D., 2007. One path to acoustic cloaking. New J. Phys. 9, 45.
Diatta, A., Guenneau, S., 2014. Controlling solid elastic waves with spherical cloaks. Appl. Phys. Lett. 105, 021901.
Farhat, M., Guenneau, S., Enoch, S., 2009a. Ultrabroadband elastic cloaking in thin plates. Phys. Rev. Lett. 103, 024301.
Farhat, M., Guenneau, S., Enoch, S., 2012. Broadband cloaking of bending waves via homogenization of multiply perforated radially symmetric and isotropic thin elastic plates. Phys. Rev. B 85, 020301.
Farhat, M., Guenneau, S., Enoch, S., Movchan, A.B., 2009b. Cloaking bending waves propagating in thin elastic plates. Phys. Rev. B 79, 033102.
Frenzel, T., Kadic, M., Wegener, M., 2017. Three-dimensional mechanical metamaterials with a twist. Science 358, 1072–1074.
Greenleaf, A., Lassas, M., Uhlmann, G., 2003a. Anisotropic conductivities that cannot be detected by EIT. Physiol. Meas. 24, 413–419.
Greenleaf, A., Lassas, M., Uhlmann, G., 2003b. On nonuniqueness for Calderón's inverse problem. Math. Res. Lett. 10, 685–693.
Hadjesfandiari, A.R., Dargush, G.F., 2011. Couple stress theory for solids. Int. J. Solids Struct. 48, 2496–2510.
He, Q.C., Zheng, Q.S., 1996. On the symmetries of 2d elastic and hyperelastic tensors. J. Elast. 43, 203–225.
Leonhardt, U., 2006. Optical conformal mapping. Science 312, 1777–1780.
Li, J., Pendry, J.B., 2008. Hiding under the carpet: a new strategy for cloaking. Phys. Rev. Lett. 101, 1–4.
Liu, X.N., Huang, G.L., Hu, G.K., 2012. Chiral effect in plane isotropic micropolar elasticity and its application to chiral lattices. J. Mech. Phys. Solids 60, 1907–1921.
Maugin, G., 1998. On the structure of the theory of polar elasticity. Philos. Trans. R. Soc. A Math. Phys. Eng. Sci. 356, 1367–1395.
Milton, G.W., Briane, M., Willis, J.R., 2006. On cloaking for elasticity and physical equations with a transformation invariant form. New J. Phys. 8, 248–267.
Mindlin, R.D., 1963. Influence of couple-stresses on stress concentrations. Exp. Mech. 3, 1–7.
Mindlin, R.D., Tiersten, H.F., 1962. Effects of couple-stresses in linear elasticity. Arch. Ration. Mech. Anal. 11, 415–448.
Nassar, H., Chen, Y., Huang, G.L., 2018. A degenerate polar lattice for cloaking in full two-dimensional elastodynamics and statics. Proc. R. Soc. A 474, 20180523.
Norris, A.N., 2008. Acoustic cloaking theory. Proc. R. Soc. A 464, 2411–2434.
Norris, A.N., 2012. Comment on "design of acoustic devices with isotropic material via conformal transformation" [appl. phys. lett. 97, 044101 (2010)]. Appl. Phys. Lett. 100, 066101.
Norris, A.N., 2015. Acoustic cloaking. Acoust. Today 11, 38–46.
Norris, A.N., Parnell, W.J., 2012. Hyperelastic cloaking theory: transformation elasticity with pre-stressed solids. Proc. R. Soc. A 468, 2881–2903.
Norris, A.N., Shuvalov, A.L., 2011. Elastic cloaking theory. Wave Motion 48, 525–538.
Parnell, W.J., 2012. Nonlinear pre-stress for cloaking from antiplane elastic waves. Proc. R. Soc. A 468, 563–580.
Parnell, W.J., Norris, A.N., Shearer, T., 2012. Employing pre-stress to generate finite cloaks for antiplane elastic waves. Appl. Phys. Lett. 100, 171907.
Pendry, J.B., Schurig, D., Smith, D.R., 2006. Controlling electromagnetic fields. Science 312, 1780–1782.
Rosi, G., Auffray, N., 2016. Anisotropic and dispersive wave propagation within strain-gradient framework. Wave Motion 63, 120–134.
Spadoni, A., Ruzzene, M., 2012. Elasto-static micropolar behavior of a chiral auxetic lattice. J. Mech. Phys. Solids 60, 156–171.
Spadoni, A., Ruzzene, M., Gonella, S., Scarpa, F., 2009. Phononic properties of hexagonal chiral lattices. Wave Motion 46, 435–450.
Stenger, N., Wilhelm, M., Wegener, M., 2012. Experiments on elastic cloaking in thin plates. Phys. Rev. Lett. 108, 014301.
Toupin, R.A., 1964. Theories of elasticity with couple-stress. Arch. Ration. Mech. Anal. 17, 85–112.
Xu, L., Chen, H., 2014. Conformal transformation optics. Nat. Photonics 9, 15–23.